8.A.8 Nuclear Physics B14 (1969) 91-105. North-Holland Publ. Comp., Amsterdam

NEW EXPERIMENTAL RESULTS ON THE REACTIONS $K^-p \to \bar{K}N$ AND $K^-p \to \Sigma\pi$ AND A PARTIAL-WAVE ANALYSIS BETWEEN 430 AND 800 MeV/c

R. ARMENTEROS, P. BAILLON, C. BRICMAN*, M. FERRO-LUZZI, D. E. PLANE and N. SCHMITZ**
CERN, Geneva

E. BURKHARDT, H. FILTHUTH, E. KLUGE‡, H. OBERLACK and R. R. ROSS‡‡
Institut für Hochenergiephysik, Heidelberg

R. BARLOUTAUD, P. GRANET, J. MEYER, J. P. PORTE and J. PREVOST
CEN, Saclay

Received 25 August 1969

Abstract: The reactions $K^-p \to K^-p$, $\bar{K}^0n$ and $K^-p \to \Sigma^+\pi^-$, $\Sigma^0\pi^0$, $\Sigma^-\pi^+$ have been studied in the c.m. energy range 1530 - 1700 MeV; new experimental data are presented and results of an energy-dependent partial-wave analysis are discussed.

1. INTRODUCTION

The reactions

$$K^-p \to K^-p \quad (1a)$$
$$\to \bar{K}^0n \quad (1b)$$
$$\to \Sigma^+\pi^- \quad (2a)$$
$$\to \Sigma^-\pi^+ \quad (2b)$$
$$\to \Sigma^0\pi^0 \quad (2c)$$

have been studied in the momentum range 430 - 800 MeV/c, where strange

* Visitor from I.I.S.N., Bruxelles.
** Present address: Max-Planck-Institut für Physik und Astrophysik, München.
‡ Present address: Stanford Linear Accelerator Centre, Stanford, Cal.
‡‡ Present address: Lawrence Radiation Laboratory, University of California, Berkeley, California.

hyperon resonances with masses between 1530 and 1700 MeV can be formed. This experiment extends our analysis of the $\bar{K}N$ interaction [1, 2] to lower energies and includes new data at 8 momenta between 430 and 600 MeV/c. Partial and differential cross sections, together with Σ^+ and Σ^0 polarizations, have been measured at $\approx$ 20 MeV/c intervals throughout the region.

As a result of energy-dependent partial-wave analyses, performed separately on the $\bar{K}N$ and $\Sigma\pi$ channels, we do not find evidence for any new resonant states in this energy region; however this does not exclude the existence of resonances weakly coupled to the above channels or resonances which defy the parametrization used. The partial-wave amplitudes reported here are found to be continuous with those at higher energies [1, 2] and with preliminary results of an experiment at lower energies [3], indicating that our parametrization provides an adequate approximation.

2. DATA

This investigation continues our analysis of K^-p interactions and includes both data from a previously reported experiment [1, 2] and new data points from 430 to 600 MeV/c. In addition, new data at 773 and 793 MeV/c has been obtained specifically to provide overlap between exposures at different times. The new data derive from an exposure of the 81-cm hydrogen bubble chamber at the CERN PS to a separated K^- beam [4] at 10 different incident momenta. A total of 200 000 pictures were taken, with an average of 7 K^- per picture except at the lowest momenta, where the K^- flux dropped considerably. At 436 MeV/c there were about 2.7 K^- per picture. For each momentum setting the central value of the K^- incident momentum at the chamber entrance was determined to an accuracy of ± 1 MeV/c by measuring and fitting τ-decays. After unfolding measurement errors, a spread of $\pm 1\%$ was found at all momenta. For each event a weighted average of the measured momentum and that found by extrapolating the above central value to the interaction point, was introduced as starting value into the kinematical fitting programme GRIND.

All events were required to be in a restricted fiducial volume, chosen so that events could be well measured and clearly visible. The K^- pathlength was determined, for all reactions except (1a), by counting the τ-decays found in the same fiducial volume. The films were all doubly scanned.

2.1. *The reaction* $K^-p \to K^-p$

At the 10 different momenta, about 100 000 pictures were scanned for events of the two-prong topology yielding 14 500 K^-p elastic scatterings. The method used for analysing these events are those described in ref. [1]. In particular, the elastic cross sections are found using a K^- path length determined by counting beam tracks. Several corrections have been applied:

(i) The beam contamination due to muons and pions varied with momentum from 10 to 15%, except at the lowest momentum where it was 28%.

(ii) The attenuation of the beam due to K^-p interactions and K^- decays was $\approx 6\%$ for high and $\approx 10\%$ for low momenta respectively.
(iii) The scanning losses due to a small projected length of the recoil proton were corrected as described in ref. [1]. On the other hand, the momentum transfer to the recoil proton is so small for forward scattering and therefore losses are so big that only events with c.m.s. $\cos\theta < 0.95$ could be accepted for beam momenta less than 0.6 GeV/c. For these events the average detection efficiency was 97%.
(iv) A correction of $\approx 1\%$ for kinematical ambiguities between π^-p and K^-p forward elastic scattering has been applied.
(v) Approximately 2% of the events could not be finally analysed. These events were accounted for by assuming the same distribution among the final states as for the fitted events.

2.2. *The reaction* $K^-p \to \bar{K}^0n$

Out of $\approx$ 7900 events of the topology zero-prong V^0, approximately 1600 were found to belong to reaction (1b), with the visible decay $K_1^0 \to \pi^+\pi^-$. There is clearly a loss for those K_1^0 which decay outside the chamber, and for those which decay close to the interaction vertex. The projected path of the decaying particle was required to be greater than 2 mm. The above losses were then compensated by weighting each remaining event by the inverse of the probability that the K_1^0 decayed in the fiducial volume with a projected length longer than the above value. Other biases, which were found, have a negligible influence on the results. They will be described in ref. [5]. The unobserved decay modes were accounted for, using $K_1^0 \to \pi^+\pi^-/\bar{K}^0 \to \text{all} = \frac{1}{3}$.

2.3. *The reactions* $K^-p \to \Sigma^\pm\pi^\mp$

The films were scanned for events appearing as two emerging charged tracks, with a kink in one of them corresponding to a possible sigma decay. Losses due to short sigmas and escape from the fiducial volume are treated in the same way as for the K_1^0 decays. For the decay mode $\Sigma^+ \to p\pi^0$, further visual biases occur. There is a loss of events having a small decay angle between the proton and the sigma. This is treated by demanding the laboratory decay-angle to be greater than 8^0, then transforming this angle into the sigma rest frame and weighting each event by the inverse of its detection probability. A loss due to short protons was similarly corrected. A further bias still exists for events having small azimuthal angles between the sigma decay plane and the direction perpendicular to the plane containing the line of sight and the sigma momentum. The effect of this bias is to destroy the uniformity expected for the distribution of this angle. Each event was appropriately weighted to compensate for this loss. Evidence that the above corrections indeed compensate for the losses will be presented in ref. [5]. Average total weights were 1.23 for Σ^+ and 1.16 for Σ^-. Finally, for K^- momenta less than 600 MeV/c, an experimentally determined cut was made in the c.m.s. angular distributions in order to eliminate all sigmas which could have a range less than 2 mm. The Legendre polynomial coefficients were then determined on these cut distributions

using eqs. 3 and 4 of subsect. 2.5 below. The new data consist of 4800 reactions (2a) and 3400 reactions (2b).

2.4. *The reaction* $K^-p \to \Sigma^0\pi^0$

This interaction occurs in the zero-prong V^0 topology. On the basis of kinematical fitting (and ionization estimates when required), about 12 000 events were found to fit the reaction sequence $K^-p \to \Lambda +$ missing neutrals, $\Lambda \to p\pi^-$. A minimum projected Λ-trajectory of 2 mm was required and weights applied accordingly to account for this cut-off, for escape from the fiducial volume and for short decay protons. The overall weight is nearly constant and ≈ 1.3. The unobserved neutral decay mode of the Λ was taken into account using a branching fraction $\Lambda \to p\pi/\Lambda \to \text{all} = \frac{2}{3}$.

The cross section for the $\Sigma^0\pi^0$ events was determined as follows. A fit was made to the missing mass squared (MM^2) distribution at the production vertex by allowing the contributions of the final states $\Lambda\pi^0$, $\Sigma^0\pi^0(\Sigma^0 \to \Lambda\gamma)$, $\Lambda\pi^0\pi^0$ and $\Lambda\eta$ to be varied. To include the effect of measurement errors, gaussian distributions were assumed for the π^0 and η peaks; the rectangular distribution for the $\Sigma^0\pi^0$ events, for which MM is the $\pi^0\gamma$ effective mass, was similarly modified. The $\Lambda\pi^0\pi^0$ contribution was described by a phase-space spectrum. The fit then gave the fraction of events contributing to the different final states and hence the cross sections. An example of such a fit can be seen in fig. 1, for an incident K^- momentum of 740 MeV/c.

In order to find the angular distributions, two problems have to be solved. As neither the Σ^0 nor the π^0 are seen directly, the production angle of the Σ^0 is taken to be that of the Λ from Σ^0 decay. At our momenta, the smearing effect introduced here is generally less than the bin width in which these events are histogrammed ($d\cos\theta = 0.2$). The second problem is how to separate the $\Sigma^0\pi^0$ events from the other reactions. Cuts were made

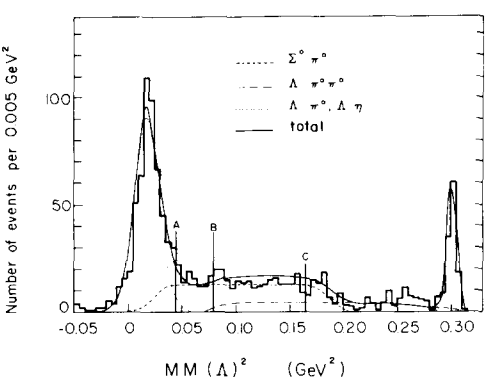

Fig. 1. Missing-mass squared distribution for the reaction $K^-p \to \Lambda +$ MM at the K^- incident momentum 740 MeV/c. The contributions of the $\Lambda\pi^0$, $\Sigma^0\pi^0$, $\Lambda\pi^0\pi^0$ and $\Lambda\eta$ final states, obtained as described in the text, are shown by the curves. The lines A, B and C indicate the cuts, described in subsect. 2.4., used in the $\Sigma^0\pi^0$ analysis.

in the MM^2 distribution and all events lying between the limits were attributed to $\Sigma^0\pi^0$. Two sets of cuts were tried, illustrated, for the incident K^- momentum of 740 MeV/c, in fig. 1. In both cases the lower cut (cut A) was chosen to exclude all but a negligible contamination of $\Lambda\pi^0$ events. The upper cut was chosen either to eliminate the $\Lambda\pi^0\pi^0$ events (cut B), or to extend to the limit of the MM^2 range for $\Sigma^0\pi^0$ (cut C), thus increasing the statistics at the expense of a certain contamination of $\Lambda\pi^0\pi^0$ events. Legendre polynomials (see below) were then fitted to the angular distribution and the values of the normalised coefficients compared for the two cuts. The results in general were in agreement within the large statistical errors, so the upper cut was fixed at the higher value, cut C. In this way a total of 4000 $\Sigma^0\pi^0$ events was obtained in the region from 436 to 800 MeV/c.

2.5. *Expansion in Legendre polynomials*

For all reactions, the c.m. angular and (when available) polarization distributions were fitted at each momentum to the following expansions:

$$d\sigma/d\Omega = \lambda\!\!\!^{-2} \sum_n A_n P_n(\cos\theta) \tag{3}$$

$$\boldsymbol{P}\frac{d\sigma}{d\Omega} = \hat{\boldsymbol{n}}\lambda\!\!\!^{-2} \sum_n B_n P_n^1(\cos\theta) \ , \tag{4}$$

where $P_n(\cos\theta)$ and $P_n^1(\cos\theta)$ are the Legendre and first-associated Legendre polynomials, θ is the c.m. angle between incoming and outgoing meson, and $\lambda\!\!\!^{-}$ is the c.m. wavelength of the incident channel. The normal $\hat{\boldsymbol{n}}$ to the production plane is defined as $\hat{\boldsymbol{n}} = (\hat{\boldsymbol{K}} \times \hat{\boldsymbol{\pi}})/|\hat{\boldsymbol{K}} \times \hat{\boldsymbol{\pi}}|$. The polarization $\boldsymbol{P}$ of the Σ^+ in reaction (2a) is determined from the decay distribution $(1 + \alpha P \cos\zeta)$ for $\Sigma^+ \to p\pi^0$, where ζ is the angle between the normal to the prosuction plane and the decay proton in the Σ^+ rest system, and $\alpha = -1$. The polarization of the Σ^0, $\boldsymbol{P} = -3\boldsymbol{P}_\Lambda$, follows from the polarization $\boldsymbol{P}_\Lambda$ of the Λ in the decay $\Sigma^0 \to \Lambda\gamma$. The polarization $\boldsymbol{P}_\Lambda$ is obtained from the decay distribution $(1 + \alpha_\Lambda P_\Lambda \cos\phi)$ of $\Lambda \to p\pi$, ϕ being the angle between the proton in the Λ rest system and the normal to the plane containing the directions of the incident K and the Λ; $\alpha_\Lambda = 0.65$.

For a good fit, it was sufficient to use an expansion including the 4th order term, the higher coefficients being compatible with zero. Figs. 2 to 4 give the obtained coefficients: figs. 2 and 3 show, as functions of the lab momentum, the A-coefficients for the $\bar{K}N$ and $\Sigma\pi$ channels (1) and (2) respectively and fig. 4 the B-coefficients for reactions (2a) and (2c). These coefficients were used as the input experimental data for an energy-dependent partial-wave analysis, carried out for the $\bar{K}N$ and $\Sigma\pi$ channels separately. Experimental values for the total K^-p cross section σ_T and for the total $\bar{K}N$ cross sections σ_0 and σ_1 in the $I = 0$ and $I = 1$ state respectively, were included in the $\bar{K}N$ analysis via the optical theorem; they are shown in fig. 5. The cross-section values above 600 MeV/c were obtained from counter measurements [6] by interpolation to our momenta. Below 600 MeV/c, where no counter measurements are available, the values used for σ_T were those obtained in this experiment [5].

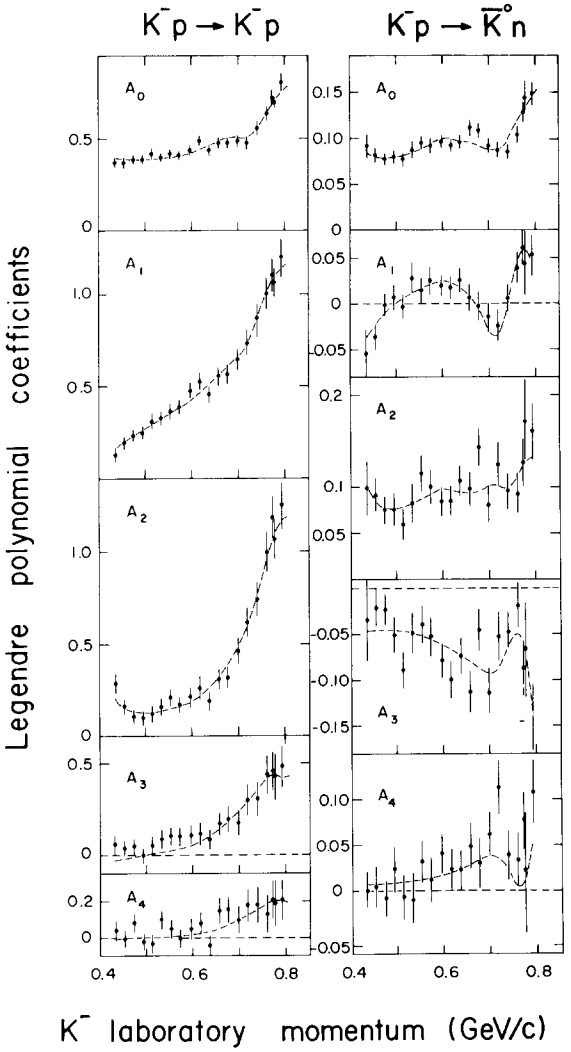

Fig. 2. Coefficients A_n of the Legendre polynomial expansion (3) for the reactions $K^-p \to \bar{K}N$, versus K^- laboratory momentum. The curves represent the best fit with the parameters of table 1.

There are 231 independent data points for the $\bar{K}N$ channel (taking into account the relation $\sigma_T = \frac{1}{2}(\sigma_0 + \sigma_1)$) and 478 data points for the $\Sigma\pi$ channel.

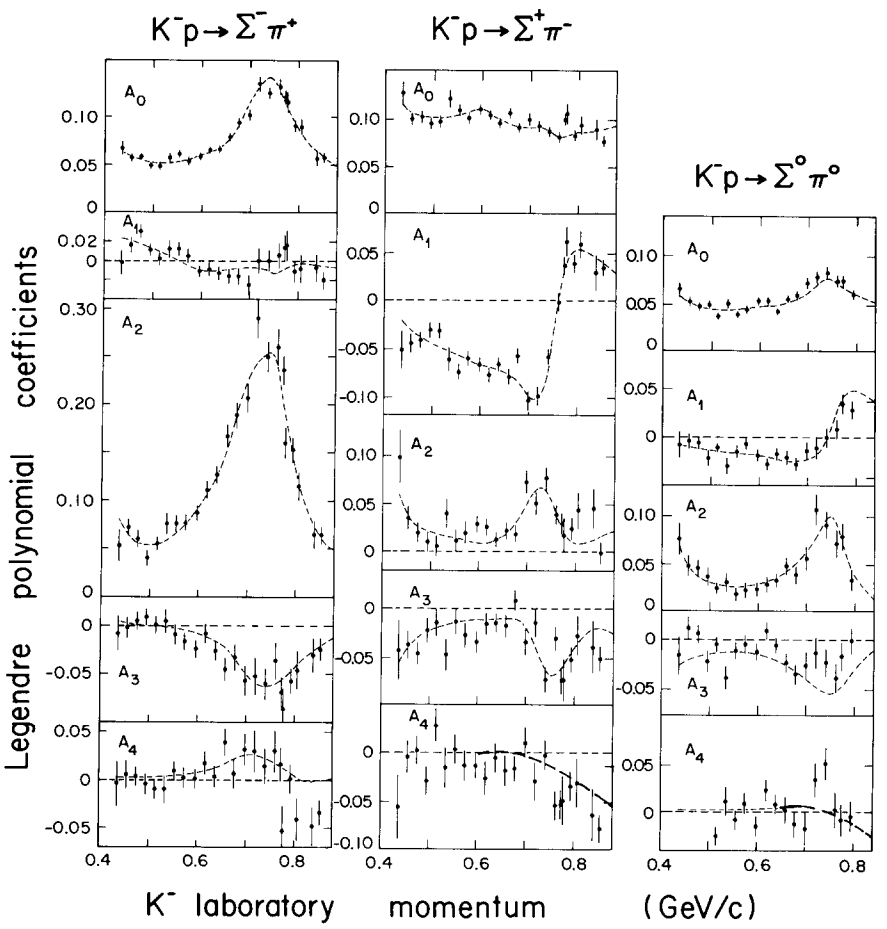

Fig. 3. Coefficients A_n of the Legendre polynomial expansion (3) for the reactions $K^-p \to \Sigma\pi$, versus K^- laboratory momentum. The curves represent the best fit with the parameters of table 2.

3. PARTIAL-WAVE ANALYSIS AND RESULTS

The convention used for the partial waves T_l is that described in ref. [7] and is based on the following expansions of the non-spin-flip (f) and the spin-flip (g) amplitudes in terms of Legendre polynomials:

$$f(\theta) = \lambda \sum [(l+1)T_l^+ + lT_l^-]P_l(\cos\theta) ,$$

$$g(\theta) = i\lambda \sum [T_l^+ - T_l^-]P_l^1(\cos\theta) .$$

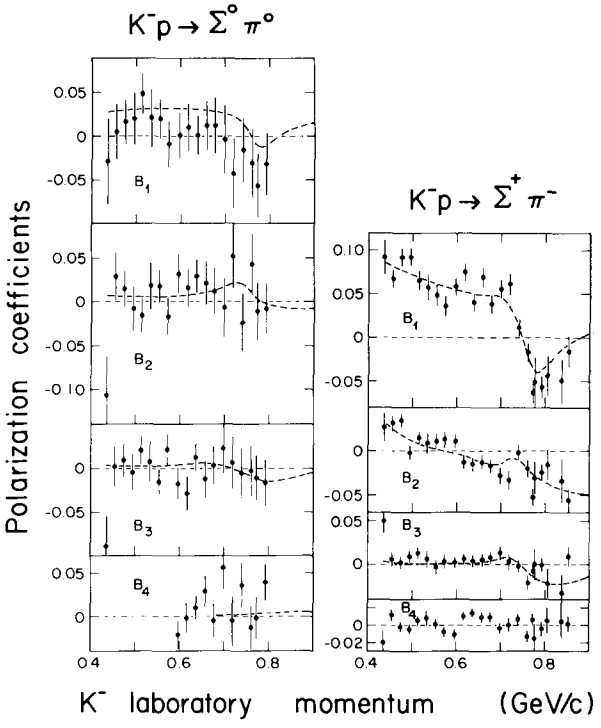

Fig. 4. Coefficients B_n of the polynomial expansion (4) for the polarization of the reactions $K^-p \to \Sigma^{\pm}\pi^{\mp}$. The curves represent the best fit with the parameters of table 2.

An energy-dependent partial-wave analysis has been made. Clearly, since the energy dependence of the amplitude is unknown, any parametrization introduced must be an approximation and so we only expect to fit the major features displayed by the data.

Each partial-wave amplitude was assumed to be either background, resonant or a superposition of both. The following parametrizations have been used to express the energy dependence:

(i) Background amplitdues, T_b: each amplitude was approximated by two straight lines in the Argand diagram, depending linearly on the lab. momentum p_K and joining together at 0.6 GeV/c:

$$T_b = a + b_1(p_K - 0.6) \qquad \text{for } p_K > 0.6 \text{ GeV}/c\ ,$$

$$T_b = a + b_2(p_K - 0.6) \qquad \text{for } p_K < 0.6 \text{ GeV}/c\ .$$

The complex numbers a, b_1 and b_2 are the free parameters to be adjusted to the data with the constraint that T_b is always inside the unitary circle.

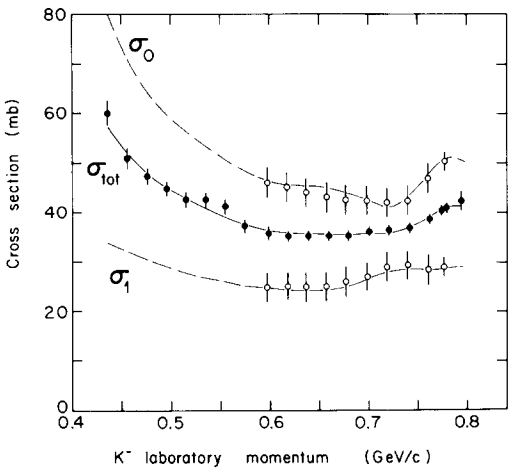

Fig. 5. K^-p total cross section σ_{tot} and $\bar{K}N$ cross sections σ_0 and σ_1 for the $I=0$ and $I=1$ states. The data above 0.6 GeV/c are obtained by interpolation from ref. [6] with errors assigned so to account also for possible systematic differences. Data below 0.6 GeV/c come from this experiment. The curves represent the solution with the parameters of table 1.

The joining point of the two lines has been chosen at the mid-point of our momentum range. It was felt that the introduction of more than 6 parameters per background wave would not be justified by the available statistics, whereas less than 6, as for example in a one-straight-line momentum dependence may not reproduce appropriately the behaviour of some of the amplitudes.

(ii) Resonant amplitudes, T_r: a non-relativistic Breit-Wigner formula $T_r = t/(\epsilon - i)$ was used, where $\epsilon = 2(E_r - E)/\Gamma$; E is the total c.m. energy, E_r the resonant energy and $\Gamma = \Gamma_0 B_l(E)$ the energy dependent resonance width, $t = x$ for the $\bar{K}N$ channel and $t = \pm\sqrt{xx'}$ for the $\Sigma\pi$ channel, where $x = \Gamma_{\bar{K}N}/\Gamma$ and $x' = \Gamma_{\Sigma\pi}/\Gamma$ are the branching fractions for the $\bar{K}N$ and $\Sigma\pi$ decay respectively. $B_l(E)$ is the momentum dependent part of the resonance width [7], Γ_0 being the width at resonance. The interaction radius was taken as 1 fm. The adjustable parameters are E_r, Γ_0 and t.

(iii) Superposition of background and resonance: the total partial-wave amplitude taken for the $\bar{K}N$ channel [1] was

$$T = T_b + T_r + 2i T_b T_r$$

and for the $\Sigma\pi$ channel

$$T = T_b + T_r \,.$$

There are altogether 9 real parameters per channel to describe an amplitude in this case. The above formulation, although simplified, appears to be adequate. Different superpositions of background and resonance with the

introduction of a free phase for the resonance, were attempted. The results obtained by the two methods gave indistinguishable values within the precision of the experiment.

With the parametrization just described, one of the above three possibilities was attributed to each partial wave. For a given set of parameters, the coefficients were calculated and compared with the experimental values in figs. 2 to 5. The χ^2 resulting from this comparison was minimized by varying the parameters until the best fit was obtained in each channel.

3.1. *The* $\bar{K}N$ *channel*

An exhaustive search was made for resonances in almost all the partial waves, trying various combinations of resonant and background amplitudes parametrized as described above. No need to introduce any new resonant state was found. A good fit to the 231 data points with 43 free parameters and a χ^2 of 157 was obtained with the following assignments. The S- and P-waves were parametrized as background except for the S_{01}, for which a combination of resonance and background was taken in the form (iii) above. The resonant parameters for the higher waves, lying above the momentum region covered here, were fixed at the values found in ref. [1]; in addition, the $\Lambda(1520)$ resonance was introduced with fixed parameters as given in ref. [8]. The free parameters were those of the background amplitudes, those of the $S_{01}(1670)$ and $D_{03}(1690)$ resonances and the elasticity only of the $D_{13}(1660)$. The mass and width of $D_{13}(1660)$ were fixed at the values found in subsect. 3.2 from the $\Sigma\pi$ analysis; the elasticity found for this resonance is so small that the above parameters could not be reliably determined from the $\bar{K}N$ channel. For $\Lambda(1520)$, an energy-independent width was used. This is because the usual D-wave barrier factor, extended so far above the resonance energy, is a-priori not expected to give an adequate description of this amplitude. Furthermore it was also experimentally found that an energy-dependent width did not lead to a good fit.

The results of the fit are shown in figs. 2 and 5. The fitted parameters are given in table 1 and the Argand diagrams of the S- and P-wave amplitudes are shown in fig. 6. There is excellent agreement between the resonant parameters of table 1 and those of our previous analysis [1].

It should be noted that, although no new resonances were needed, one cannot exclude their existence with elasticities too small to show up in our data. In fig. 6, we also show the partial-wave amplitudes from our previous analysis [1] in the higher momentum range 0.6 to 1.2 GeV/c. The striking continuity between the two sets of amplitudes indicates that our parametrization for this channel is a good approximation. A similar continuity is seen between our results and those of an experiment in the region between 280 and 440 MeV/c [3], also shown in fig. 6.

3.2. *The* $\Sigma\pi$ *channel*

As for the $\bar{K}N$ channel, we fixed the parameters of the resonances lying above the momentum range at the values given in ref. [2]. Then, many combinations of resonance and background were tried in most of the partial waves in an attempt to find new resonant states. These attempt were con-

Table 1
Resonant and background parameters for the $\bar{K}N$ channel.

Non-resonant amplitudes	Re a	Im a	Re b_1	Im b_1	Re b_2	Im b_2
S_{01}	0.19 ± 0.05	0.78 ± 0.02	-0.47 ± 0.50	0.36 ± 0.45	1.33 ± 0.48	0.04 ± 0.25
S_{11}	0.05 ± 0.04	0.38 ± 0.02	0.21 ± 0.62	0.69 ± 0.25	0.29 ± 0.50	0.05 ± 0.27
P_{01}	0.17 ± 0.05	0.12 ± 0.03	-0.26 ± 0.38	1.69 ± 0.35	-0.48 ± 0.39	0.34 ± 0.43
P_{11}	-0.07 ± 0.05	0.05 ± 0.02	0.85 ± 0.37	0.19 ± 0.22	-0.60 ± 0.66	-0.38 ± 0.33
P_{03}	0.27 ± 0.03	0.11 ± 0.01	0.61 ± 0.25	0.40 ± 0.19	0.62 ± 0.33	0.15 ± 0.30
P_{13}	0.00 ± 0.03	0.07 ± 0.01	0.68 ± 0.34	-0.18 ± 0.09	-0.13 ± 0.28	0.43 ± 0.08

Resonant amplitudes	Mass E_r (MeV)	Width Γ_o (MeV)	Elasticity x
S_{01}	1662 ± 3	38 ± 15	0.14 ± 0.04
D_{03}	1691 ± 2	31 ± 7	0.18 ± 0.02
D_{03}	[1519]	[16]	[0.45]
D_{13}	[1662]	[49]	0.08 ± 0.02

The parameters in brackets have been kept fixed. The following resonances, which lie above the energy region, have been included in the analysis with fixed parameters taken from ref. [1]; $D_{05}(1807)$, $D_{15}(1768)$, $F_{05}(1817)$ and $F_{07}(1864)$. The errors are statistical only and do not contain the uncertainty arising from the chosen parametrization. The χ^2 value is 157 for 231 data points and 43 free parameters.

sistently frustrated. An acceptable fit was obtained by introducing background amplitudes in the S- and P-waves, and the following resonances lying inside the region: $S_{01}(1670)$, $D_{03}(1690)$ and $D_{13}(1660)$. Strong evidence for the S_{01} resonance in the $\Sigma\pi$ channel has already been reported [2], as well as a determination of the spin and parity of $\Lambda(1690)$ and $\Sigma(1660)$. The $\Lambda(1520)$ was treated in the same way, and for the same reasons, as in the $\bar{K}N$ channel. Resonant parameters obtained in this fit closely resemble those published in ref. [2].

In table 2 we give the parameters resulting from the best fit. The χ^2 was 647 for 478 data points and 45 variable parameters. Despite this high χ^2 value, which could be due to an underestimate of errors or a more complicated energy dependence of the amplitudes, the fitted curves shown in figs. 3 and 4 do reproduce the gross features of the data. The Argand

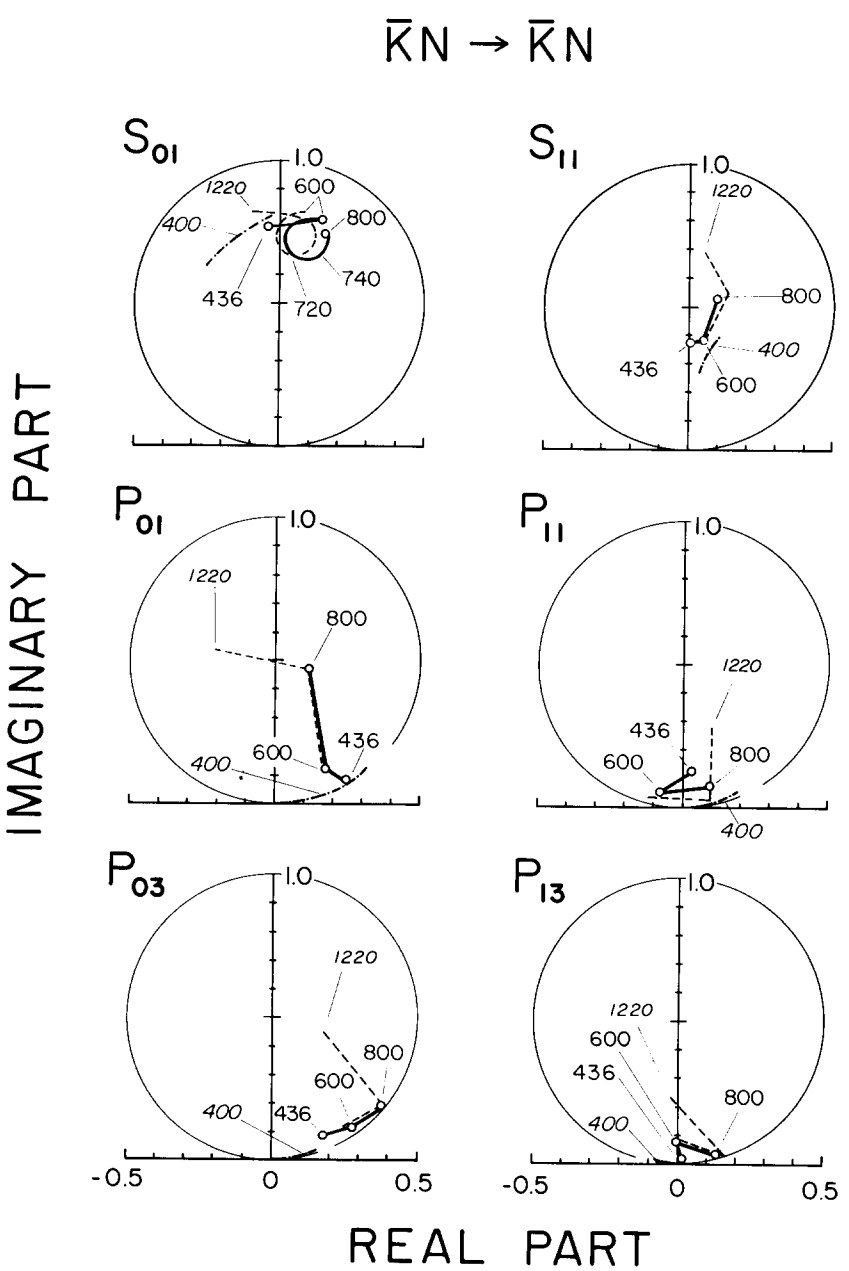

Fig. 6. Argand diagrams of the S- and P-waves for the reaction $\bar{K}N \rightarrow \bar{K}N$. The full lines represent the solution of table 1. The K^- laboratory momentum is given in MeV/c. The dashed lines represent the solution for the higher momentum range, 0.6 - 1.2 GeV/c [1]. The dot-dashed curves (marked 400) are the solution of ref. [3], between 0.28 - 0.44 GeV/c.

Table 2
Resonant and background parameters for the $\Sigma\pi$ channel.

Non-resonant amplitudes	Re a	Im a	Re b_1	Im b_1	Re b_2	Im b_2
S_{01}	0.26 ± 0.02	- 0.29 ± 0.03	- 0.32 ± 0.19	0.77 ± 0.20	- 0.31 ± 0.04	- 0.05 ± 0.05
S_{11}	0.13 ± 0.03	0.33 ± 0.02	- 0.48 ± 0.18	- 0.85 ± 0.20	0.00 ± 0.20	0.22 ± 0.22
P_{01}	0.01 ± 0.02	0.17 ± 0.04	- 0.57 ± 0.17	0.45 ± 0.29	- 0.83 ± 0.27	0.66 ± 0.45
P_{11}	0.01 ± 0.02	- 0.12 ± 0.04	0.29 ± 0.16	- 0.12 ± 0.25	0.25 ± 0.23	- 1.12 ± 0.39
P_{03}	- 0.10 ± 0.02	- 0.09 ± 0.03	- 0.17 ± 0.12	- 0.04 ± 0.17	0.14 ± 0.22	- 0.60 ± 0.30
P_{13}	0.06 ± 0.02	- 0.04 ± 0.02	0.09 ± 0.08	0.19 ± 0.11	- 0.17 ± 0.18	0.03 ± 0.20

Resonant amplitudes	Mass E_r (MeV)	Width Γ_o (MeV)	Amplitude at resonance t	Branching fraction $x_{\Sigma\pi}$
S_{01}	1680 ± 1	33 ± 5	0.30 ± 0.03	0.64 ± 0.22
D_{03}	1688 ± 2	72 ± 6	0.36 ± 0.02	0.72 ± 0.11
D_{03}	[1519]	[16]	[- 0.46]	[0.47]
D_{13}	1663 ± 2	49 ± 4	0.20 ± 0.01	0.50 ± 0.12

Parameters in brackets have been kept fixed. The errors are statistical only and do not include the uncertainty arising from the chosen parametrization. Resonances in the D_{05}, D_{15} and F_{05} waves have been included in the analysis with the fixed parameters of ref. [2]. A positive (negative) sign for t describes a resonant amplitude in the direction of the positive (negative) imaginary axis. The χ^2 value is 647 for 478 data points and 45 variable parameters.

diagrams of fig. 7 show the S- and P-waves, compared with those obtained in the earlier analysis of the momentum range 0.6 to 1.0 GeV/c [2]. Also shown, and in good agreement, are the results of an analysis of the region 280 - 440 MeV/c [3].

4. CONCLUSIONS

No evidence was found for the existence of hyperon resonances with masses between 1530 and 1600 MeV. Within the precision of the experiment we would have detected resonant states with a coupling to the $\bar{K}N$ or the $\Sigma\pi$ channel giving rise to amplitudes at resonance, t, larger than ≈ 0.10.

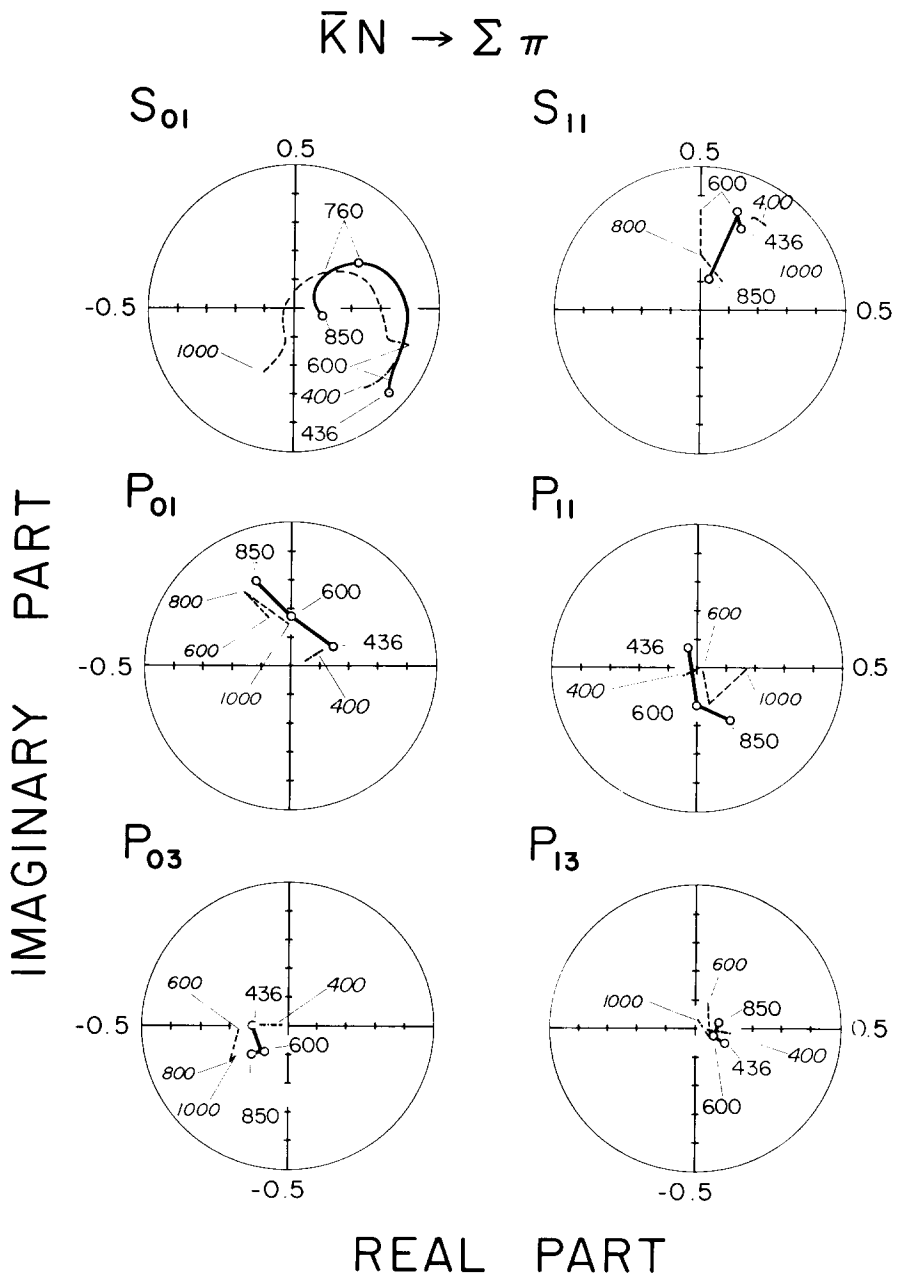

Fig. 7. Argand diagrams of the S- and P-waves for the reaction $\bar{K}N \rightarrow \Sigma\pi$. The K^- laboratory momentum is given in MeV/c. The full lines represent the solution of table 2, whereas the dashed lines represent the solution for the higher momentum range, 0.6 - 1.0 GeV/c [2]. The dot-dashed curves (marked 400) are the solution of ref. [3], between 0.28 - 0.44 GeV/c.

The amplitudes obtained for the momentum region between 436 and 600 MeV/c appear to join smoothly with those in the neighbouring regions [1 - 3] thereby adding to the confidence in the method and in the approximations introduced.

REFERENCES

[1] R. Armenteros, P. Baillon, C. Bricman, M. Ferro-Luzzi, D.E. Plane, N. Schmitz, E. Burkhardt, H. Filthuth, E. Kluge, H. Oberlack, R.R. Ross, R. Barloutaud, P. Granet, J. Meyer, J.P. Porte and J. Prevost, Nucl. Phys. B8 (1968) 195; B10 (1969) 432.
[2] R. Armenteros, P. Baillon, C. Bricman, M. Ferro-Luzzi, D.E. Plane, N. Schmitz, E. Burkhardt, H. Filthuth, E. Kluge, H. Oberlack, R.R. Ross, R. Barloutaud, P. Granet, J. Meyer, J.P. Porte and J. Prevost, Nucl. Phys. B8 (1968) 223.
[3] A. Barbaro-Galtieri, M. Alston-Garnjost, R.O. Bangerter, L.K. Gershwin, T.S. Mast and R.D. Tripp, Branching rations of $\Lambda(1520)$, presented at the Lund conference on elementary particles (1969).
[4] D.E. Plane and P. Lexa, CERN PS users handbook, L 85 (1967).
[5] R. Armenteros, P. Baillon, C. Bricman, M. Ferro-Luzzi, J.O. Petersen, D.E. Plane, N. Schmitz, E. Burkhardt, H. Filthuth, E. Kluge, H. Oberlack, R.R. Ross, R. Barloutaud, P. Granet, J. Meyer, J.P. Porte and J. Prevost, Data analysis of K^-p interactions between 436 - 800 MeV/c, to be published.
[6] R.L. Cool, G. Giacomelli, T.F. Kycia, B.A. Leontic, K.K. Li, A. Lundby and J. Teiger, Phys. Rev. Letters 16 (1966) 1228;
D.V. Bugg, R.S. Gilmore, K.M. Knight, D.C. Salter, G.H. Stafford, E.J.N. Wilson, J.D. Davies, J.D. Dowell, P.N. Hattersley, R.J. Homer, A.W. O'Dell, A.A. Carter, R.J. Tapper and K.F. Riley, Phys. Rev. 168 (1968) 1466.
[7] R.D. Tripp; Baryon resonances Proc. int. school of physics, Varenna 1964 (Academic Press, New York).
[8] Particle Data Group; Revs. Mod. Phys. 41 (1969) 109.